SENSING AND SEALING OF MEMBRANE DAMAGE BY ANNEXIN A4

Andrea Erlbruch[*], Alen Piljić[*], Charlotta Funaya[†], Zsófia Seboe-Lemke[†1], Claude Antony[†] , Carsten Schultz[*]

Cell Biology and Biophysics Unit[*] and Electron Microscopy Core Facility[†],

European Molecular Biology Laboratory (EMBL), Meyerhofstr. 1,

69117 Heidelberg, Germany

[1] present address: Chiltern International GmbH, 61325 Bad Homburg v.d.H., Germany

Corresponding author: Carsten Schultz (Schultz@embl.de), *Cell Biology and Biophysics Unit, European Molecular Biology Laboratory (EMBL), Meyerhofstr. 1,*

69117 Heidelberg, Germany, Tel: +49 6221-387-210, Fax: +49 6221-387-206

Running title: Translocation phenomena in membrane repair

Key words: annexin, imaging, electron microscopy, membrane repair, translocation,

ABSTRACT

Cell wounding is commonly accompanied by a rupture of the plasma membrane. To protect cells against the sustained loss of cytoplasm and a pathological increase in $[Ca^{2+}]_{i,}$ a rapid and effective repair machinery has to be activated to reseal the impact site. By live cell multiparamter imaging, we showed that after membrane damage, several Ca^{2+}-effectors, such as annexins or PKC are recruited to the impact site in a highly spatio-temporally coordinated manner. We identified several annexins as components of the initial phase in the sealing process, but acting on the membranes independently and with different tasks. Corresponding with successful repair, annexin A4 was by far the fastest molecule to accumulate and to self-associate at the lesion,. Correlative electron-microscopy revealed annexin A4 localization in the region of the impact. We conclude, that annexin A4 senses membrane damage, suggesting an important role in this pivotal cellular process.

INTRODUCTION

Plasma membrane ruptures provoked by mechanical forces are a common form of cellular injury for many different eukaryotic/mammalian cell types under normal physiological conditions (McNeil and Kirchhausen, 2005; McNeil and Terasaki, 2001). Cell types known to be regularly exposed to membrane ruptures are skeletal and cardiac muscle cells (Clarke et al., 1995; McNeil and Khakee, 1992), epidermal cells, epithelia as well as endothelia cells (McNeil and Ito, 1989; McNeil et al., 1989; Yu and McNeil, 1992). The rupture of the plasma membrane is a major threat to the viability of a cell, mainly through the strong influx of extracellular calcium (Bement et al., 2007). Increased Ca^{2+} levels evoke an enormous number of intracellular events and ultimately lead to apoptosis when persisting over longer periods of time (Lemasters et al., 1987; Orrenius et al., 2003). Therefore, the rapid sealing of plasma membranes is crucial to prevent the loss of cytoplasm and to ensure cell survival. Membrane ruptures are particularly common in muscle cells and defects in genes of proteins involved in membrane repair lead to several diseases such as different forms of muscle disorders, for instance Limb Girdle Muscular Dystrophy (LGMD), Miyoshi myopathy (MM) (Bansal and Campbell, 2004; Bansal et al., 2003; Lammerding and Lee, 2007) or cardiomyopathies (Han et al., 2007; Luft, 2007). Normally, the cell is protected by a complex calcium-induced repair mechanism that involves homo- and heterotypic vesicular fusion processes to mend the rupture site, a mechanism currently described by the 'patch hypothesis' (McNeil and Kirchhausen, 2005; Terasaki et al., 1997). However, the vesicular fusion process by itself seems to be too slow and too incomplete to prevent calcium-induced damage. Therefore, calcium-

sensitive proteins that are able to form large protein assemblies on membranes are prime candidates as factors for the initial sealing event. A group of Ca^{2+}-responsive proteins are annexins which interact with anionic phospholipids, preferentially phosphatidic acid, phosphatidylserine or phosphopatidylionositol. The positive charges of the calcium ions are instrumental in the recognition of the negatively charged phospholipid headgroups. The calcium affinity in the presence of phospholipids is in the range of submicromolar to 100 μM depending on the annexin subtype (Gerke and Moss, 1997; Raynal and Pollard, 1994). In the human organism 12 different annexins (annexin A1 – A11, annexin A13) are known, differing in their tissue distribution (Dreier et al., 1998; Kaetzel et al., 1989; Kaetzel et al., 1994), in their subcellular localization (Barwise and Walker, 1996; Kaetzel et al., 1990) as well as in their biochemical properties, e.g. their affinity for Ca^{2+} or various phospholipids (Blackwood and Ernst, 1990; Raynal and Pollard, 1994). Annexins are involved in a variety of cellular processes many of them impairing membrane properties such as membrane fluidity and permeability, protein mobility, vesicle aggregation and ion homeostasis (Blackwood and Ernst, 1990; Piljic and Schultz, 2006). Structurally, all of the annexins exhibit a very similar domain organization, a conserved C-terminal protein core domain segmented by the annexin repeats and a variable N-terminal tail differing in length and amino acid sequence. Different post-translational modifications e.g. phosphorylation (Kaetzel et al., 2001; Rothhut, 1997), glycosylation (Goulet et al., 1992) or myristoylation (Wice and Gordon, 1992) of the N-terminal regions are involved in affecting the biological functions or the subcellular localization of the various annexins. In the presence of calcium ions, most of the annexins known in mammalian cells can interact with themselves to form larger assemblies at membrane

surfaces (Zaks and Creutz, 1991). Some of these assemblies, such as the one of annexin A4, are known to consist of very regular and stable trimers while others, such as annexin A1 and A2, produce more amorphous structures (Janshoff et al., 2001; Zaks and Creutz, 1991). The latter two annexin subtypes have very recently been shown to be involved in membrane repair (Babbin et al., 2008; Babbin et al., 2007; Lennon et al., 2003; McNeil et al., 2006). Although little is known about the function of annexin A1 and annexin A2 in membrane repair, the expression level of both proteins may function as a prognostic marker for LGMD and MM due to the strong correlation between high expression levels of annexin A1 and A2 and the clinical severity of such forms of muscle dystrophies (Cagliani et al., 2005).

Several methods such as ´cell scraping´ or scratching (McNeil et al., 1984; Miyake et al., 2001; Reddy et al., 2001; Swanson and McNeil, 1987), treatment of the cells with glass beads (McNeil and Warder, 1987; Miyake et al., 2001; Reddy et al., 2001), laser nanosurgery (Kohli et al., 2005; McNeil et al., 2006) or microneedle puncturing (Reddy et al., 2001; Shen and Steinhardt, 2005; Shen et al., 2005; Steinhardt et al., 1994) are commonly used for studying membrane repair (McNeil, 2001). However, only the two latter methods are controllable in timing and positioning of the impact and can be easily combined with live cell imaging. Rupturing the plasma membrane of a single cell with a pointed object for example is a very individual process with potential differences in the size and depth of the impact, even when semi-automated micromanipulators are used. Therefore, single cell imaging techniques appear to be the method of choice for studying membrane repair. In multiparameter imaging experiments, where several reporter

molecules are employed simultaneously (Piljic and Schultz, 2008; Schultz et al., 2005), the relative timing of each event is analyzed, thereby providing insight in event sequences and spatial differences of the individual responses relevant to membrane repair.

The aim of this study was to investigate the response of various annexins to a stimulatory influx of calcium by realtime imaging during a membrane-rupture protocol. By using multiparameter imaging, we were able to show the precise timing of the translocation process of calcium-sensitive proteins including annexins and protein kinase C. Annexin A4 was by far the fastest molecule of all Ca^{2+}-effectors investigated in our studies to reach the impact site. The proper accumulation of annexin A4 as well as the successful annexin A4 self-assembly correlated with effective sealing. This indicates that annexin A4 act as an intracellular sensor for recognizing membrane damage.

RESULTS

Simultaneous imaging of different annexin subtypes after wounding – The broad spectra of human annexin subtypes and isoforms, the differential expression profiles as well as different biochemical properties suggest individual functions of the annexins in different cellular processes. Although the contribution of annexin A2 and annexin A1 to plasma membrane sealing was described recently, the precise subcellular function of most annexins in this process is still unknown. Nevertheless, the inhibition of membrane resealing observed by cell-based competition assays using an annexin A1 antibody and a peptide of the N-terminus of annexin A1 as well as a Ca^{2+} binding deficient annexin A1 mutant, indicated a fundamental role of such proteins in membrane repair (McNeil et al., 2006).

In the past, we monitored simultaneously the translocation kinetics of five annexins (A1, A2, A4, A5, A6) in N1E cells after raising the intracellular calcium level by the ionophore ionomycin. Considerable differences in the timing of translocation were determined, depending on the affinity for calcium ions (Skrahina et al., 2008). Here we investigate the translocation behavior of eight annexins (A1-A7 and A9) after membrane rupture in multiparameter imaging experiment. We usually expressed three annexins transiently. Upon wounding the cells with a micromanipulator needle, we observed a rapid translocation of three annexins (A4, A1, A6 fused to mPlum, EGFP and ECFP, respectively) to the impact site with annexin A4 being by far the fastest to arrive (Figure 1 A and B, Suppl. Movie 1), followed by annexin A6 and annexin A1. The translocation was visualized by a dramatic increase in fluorescence in the area of the impact site

(Figure 1 A and B). The order of translocation correlates very well with previous experiments, where the translocation was induced by ionomycin (Skrahina et al., 2008). Due to the homogeneity of the stimulus and the maximal cellular response, ionomycin experiments are an eligible method to determine the influence of the relative annexin A4 expression level on the order of annexin translocation. By this, it was shown that a particular order of annexin subtype translocation was kept independent of the annexin expression level (Skrahina et al., 2008).

Figure 1

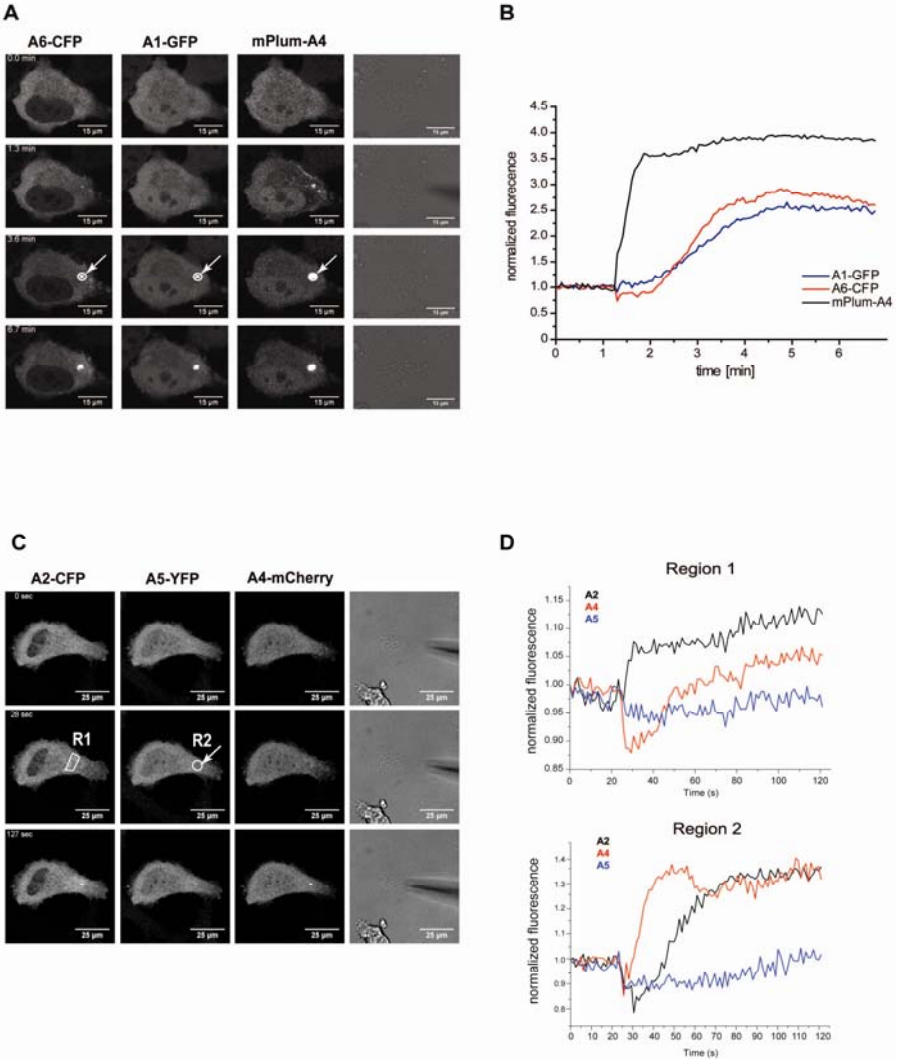

Figure 1. Simultaneous imaging of the translocation behaviour of annexin A1, annexin A2, annexin A5, annnexin A6 and annexin A4 after microneedle puncturing. (A) Time series images of a annexin A6-CFP, annexin A1-GFP and mPlum-annexin A4 co-expressing HeLa cell were acquired simultaneously after wounding the cell with a glass needle. Arrows in A indicate the impact site. Circles in A indicate the region of interest used for data analysis in graph (B). Data are representative of results obtained in 10 additional cells from 3 independent experiments. (C) Time series images of Hela cells over-expressing annexin A2-CFP, annexin A5-YFP and annexin A4-mCherry were acquired simultaneously after wounding the cell with a glassneedle. Circlular and rectangular regions indicate the regions of interest used for data analysis in (D). Annexin A4 showed the earliest response and accumulated locally at the impact site (region 2), annexin A2 accumulates in the vicinity of the impact site (region 1) and annexin A5 showed only a very weak response. Data are representative of results obtained in 8 additional cells from 3 independent experiments.

Annexin A3 and annexin A7 translocated very locally to the membrane lesion as well, but also with a slower translocation kinetic in comparison to annexin A4 (Suppl. Figure S1 A and B). Annexin A5 (Figure 1 C) showed only a very weak response and annexin A9 showed no tendency to accumulate (Suppl. Figure S1 C & D) after membrane damage.Annexin A2, however, formed assemblies in some distance from the lesion (Figure 1C). Of all annexins, A2 has the highest affinity for calcium ions (~ 0.5 μM) (Glenney, 1986). Therefore, a graded increase in $[Ca^{2+}]_i$ will be first sensed by annexin

A2, leading to phospholipid recognition distant to the impact site. In our example, a rapid increase of fluorescence was observed in a region roughly 8-15 μm from the impact, while the impact site itself only saw an accumulation of annexin A2 several minutes after the impact, likely due to some leakage of calcium through the patch (Figure 1 C and D). This result suggests that different annexins have different tasks in supporting and sealing the plasma membrane and that the complex behavior is probably a result of the various affinities for calcium ions and certain species of phospholipids. The very fast translocation of annexin A4 to the impact site of a membrane lesion led to the assumption that annexin A4 is a crucial protein of the membrane repair machinery, acting in one of the very early events of the resealing process.

Annexin A4 accumulates at the plasma membrane ruption site immediately after cellular injury – Since annexin A4 showed the most pronounced translocation effect, we focused predominantly on its role in membrane repair. A strong rise in the $[Ca^{2+}]_i$ concentration induces membrane translocation and self-association of annexin A4 molecules on membranes in living cells as was shown previously (Piljic and Schultz, 2006). Self-association of annexin A4 results in the formation of highly ordered trimer structures which most likely arranges into stable and immobile 2D-arrays (Kaetzel et al., 2001) coating the cytoplasmic site of the plasma membrane and thereby affecting the mobility of membrane proteins (Piljic and Schultz, 2006). First, we studied the behaviour of annexin A4 after injuring the plasma membrane mechanically or after ablating part of the membrane with a pulsed ultraviolet laser in combination with monitoring the Ca^{2+}-

influx. The Ca^{2+} response was measured simultaneously by loading the cells with the Ca^{2+} indicator Fluo-4. Upon wounding the cells with a blunt glass needle (Figure 2A, Suppl. Movie 2) or after a 10 sec UV laser pulse (Suppl. Figure S2), an immediate increase in the intracellular calcium concentration ($[Ca^{2+}]_i$) was observed. The spreading of the Ca^{2+} wave started at the impact site and distributed across the cell. At the same time, we measured an instantaneous and locally limited accumulation of annexin A4 to the impact site. A rapid decrease in intracellular $[Ca^{2+}]_i$ levels was observed a few seconds after wounding.

The presence of calcium is absolutely crucial for initiating a successful resealing process as e.g. shown before on sea urchin eggs (McNeil and Terasaki, 2001). For studying the calcium dependency of annexin A4 translocation to the impact site a mutant was generated, which is insensitive to a stimulatory calcium influx. Based on sequence homology studies as well as on biochemical studies five Asp/Glu residues in the annexin A4 cDNA were altered to Ala (E35A, D78A, D144A, E228A and D304A) by site directed mutagenesis (Filipenko et al., 2000; Jost et al., 1992; Nelson and Creutz, 1995). As expected, in comparison to the wildtype form of annexin A4, the calcium binding deficient mutant failed to translocate to the nuclear envelope and to the plasma membrane after ionomycin treatment (Suppl. Figure S3, A and B) or to the impact site after microneedle puncturing (Suppl. Figure S3, C). These results suggest that the local calcium influx through the membrane lesion is the prime signal for fast annexin A4 recruitment and self-association at the impact site. For visualizing annexin A4 self-association the ratiometric FRET sensor CYNEX4 (cyan-yellow-labeled annexin A4) was used (Piljic and Schultz, 2006). After membrane damage CYNEX4 accumulation at the

impact site led to a strong increase of the FRET signal (Figure 2 C and D). A slight decrease of the FRET efficiency was observed in the cytoplasm, probably due to a conformational change of the CYNEX4 sensor after membrane damage. Since annexin A4 is a substrate of PKC, it can be speculated that post-translational modifications such as phosphorylation induce a change of the intramolecular FRET efficiency. Similar structural changes were observed in vitro (Kaetzel et al., 2001).

Figure 2

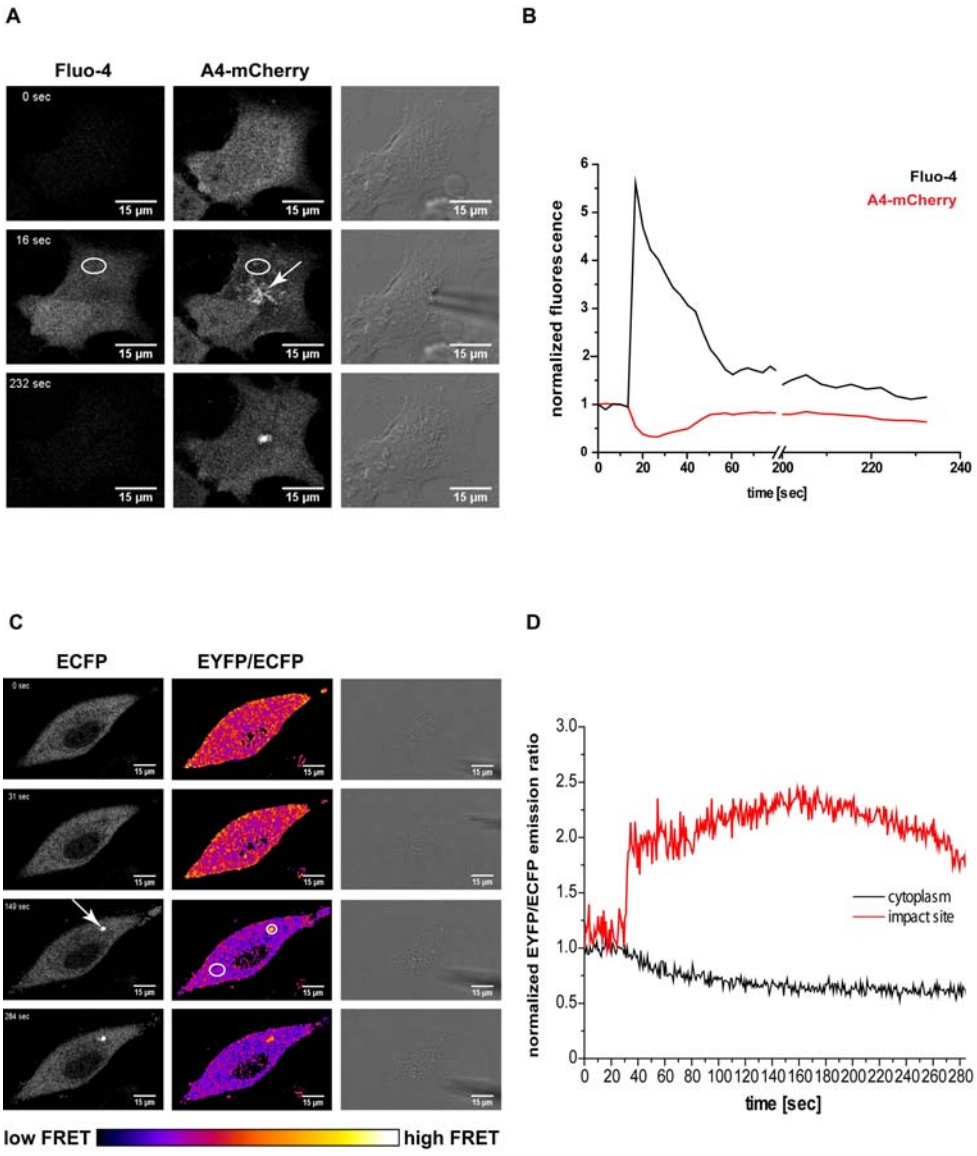

Figure 2. Annexin A4 and calcium responses after cell wounding. (A) HeLa cells expressing annexin A4-mCherry and loaded with Fluo-4 were wounded by microneedle puncturing (time point of poking t = 16 sec, arrow indicates the impact site). The increase of the emission intensity (495-520 nm) of the Ca^{2+} indicator Fluo-4 corresponds to the Ca^{2+} influx. A massive accumulation of annexin A4 at the impact site was observed in the red channel (640-700 nm). Circles show regions of interest used for Fluo-4 and mCherry emission analysis in graph (B). Data are representative of results obtained in 9 additional cells from 4 independent experiments. (C) A HeLa cell expressing CYNEX4 was wounded as described above. Time point of poking t = 31 sec. An accumulation of CYNEX4 was observed at the impact site in the CFP channel. Ratio of EYFP/ECFP emission in this region showed a significant increase in FRET. Circles show regions of interest used for data analysis in (D), arrows indicate the impact site. Data are representative of results obtained in 14 additional cells from 3 independent experiments.

Further, we addressed the question, whether annexin self-association was crucial for resealing membrane lesions. *In vitro* studies of annexin self-assembly and membrane binding showed, that both phenomena were dramatically affected by trifluorperazine (TFP), an antipsychotic drug (Zaks and Creutz, 1991).

In the presence of 120 μM TFP, annexin A4-mCherry as well as the calcium indicator Fluo-4 completely leaked from the cell in less then 30 sec after microneedle puncturing (Figure 3 A). Leakage kinetics of Fluo-4 were slightly faster in comparison to the leakage of annexin-A4 likely due to a retardation of the latter by binding to certain membrane

lipids (Figure 3 B), as is reflected by a weak fluorescence at the plasma membrane in the mCherry channel (Figure 3 A).

Figure 3

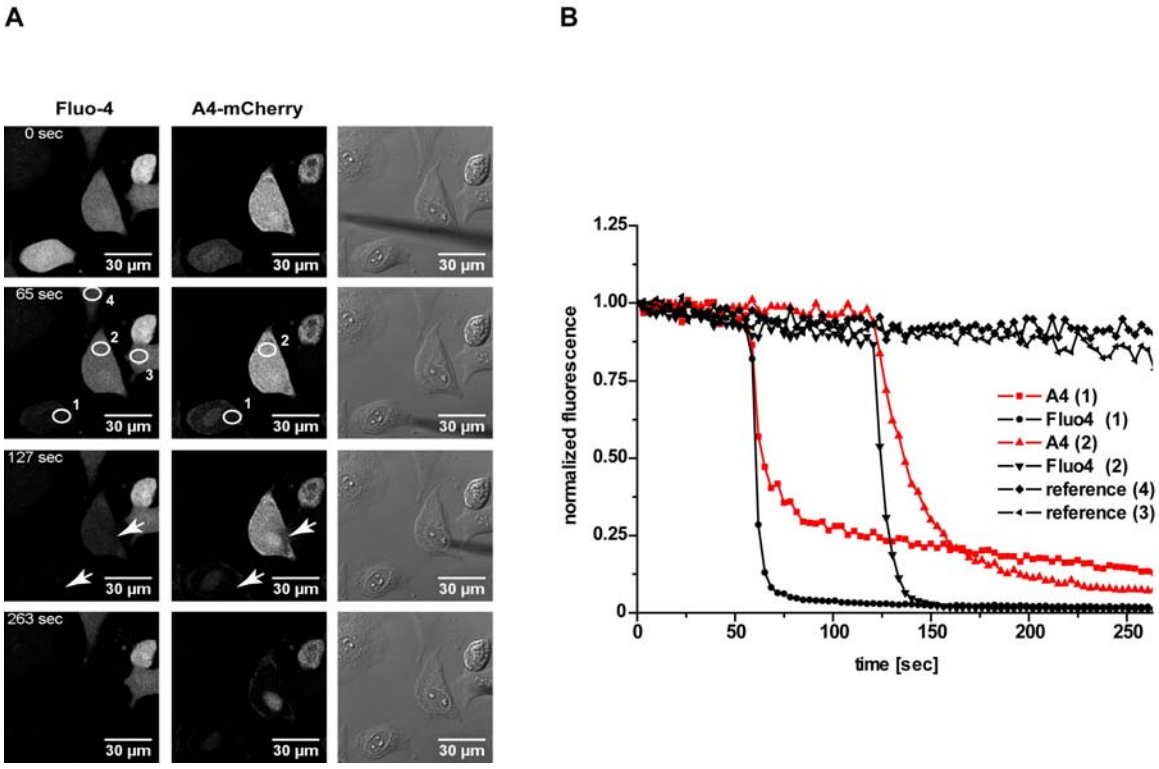

Figure 3. Failure of membrane repair in the presence of trifluorperazine (TFP). (A) HeLa cells transiently expressing annexin A4-mCherry were loaded with Fluo-4 and punctured with a glass needle in the presence of 120 µM TFP (time point of poking t = 65 sec for cell 1 and t = 127 sec for cell 2). In comparison to the reference cells (cell 3 and 4), a dramatic loss of fluorescence was observed in both channels indicative for a failure of membrane resealing. Circles show regions of interest used for data analysis in (B). (B) Traces of Fluo-4 and mCherry emission of annexin A4-mCherry expressing cells shown

in A. Data are representative of results obtained in 14 additional cells from 3 independent experiments.

Our results demonstrated that a locally limited annexin A4 translocation and self-association on membrane surfaces was induced by the strong calcium influx after membrane damage. In addition, the lack of resealing in the presence of TFP suggested that annexin A4 translocation as well as self-assembly is a crucial step in the repair process. Annexin self-association can e.g. support the repair process by providing mechanical stability by the formation of a rigid structure or by mediating membrane-membrane fusion events, a typical cellular function of many annexins (Kubista et al., 2000).

Annexin A4 accumulation at the membrane lesion prevents leakage of soluble proteins –The most crucial point after a membrane rupture is, apart from preventing the pathological increase of $[Ca^{2+}]_i$, to stop the leakage of cytoplasm. Therefore the physiologically inert fluorescent protein CFP was transiently co-expressed with annexin A4-mCherry in HeLa cells. After poking, CFP disappeared from the cytosol within a few minutes in cases where the lesion was too large to be sealed (Figure 5A, C and D). Here, annexin A4 translocation failed to be selective for the impact site but translocated to the entire plasma membrane as well as the inner leaflet of the nuclear membrane, indicative of a global increase in $[Ca^{2+}]_i$ throughout the cell (Piljic and Schultz, 2006). In contrast to

cases, where annexin A4 accumulated site-specifically to the impact site, a loss of CFP fluorescence of less than 20 % was observed in the first 30 sec after membrane damage (Figure 4B, C and D) after which a stable plateau was reached, suggesting a stop of cytoplasm leakage and sealing of the impact site (Figure 4C). The timing of loss of CFP fluorescence correlated with the drop of annexin A4 fluorescence in the cytoplasm due to membrane damage.

We conclude that (i) the locally correct accumulation of annexin A4 was essential for the rapid sealing of membrane ruptures and (ii) correlated with successful membrane repair. In contrast, when a global annexin A4 translocation to plasma and nuclear membranes was induced, resealing of the membrane failed.

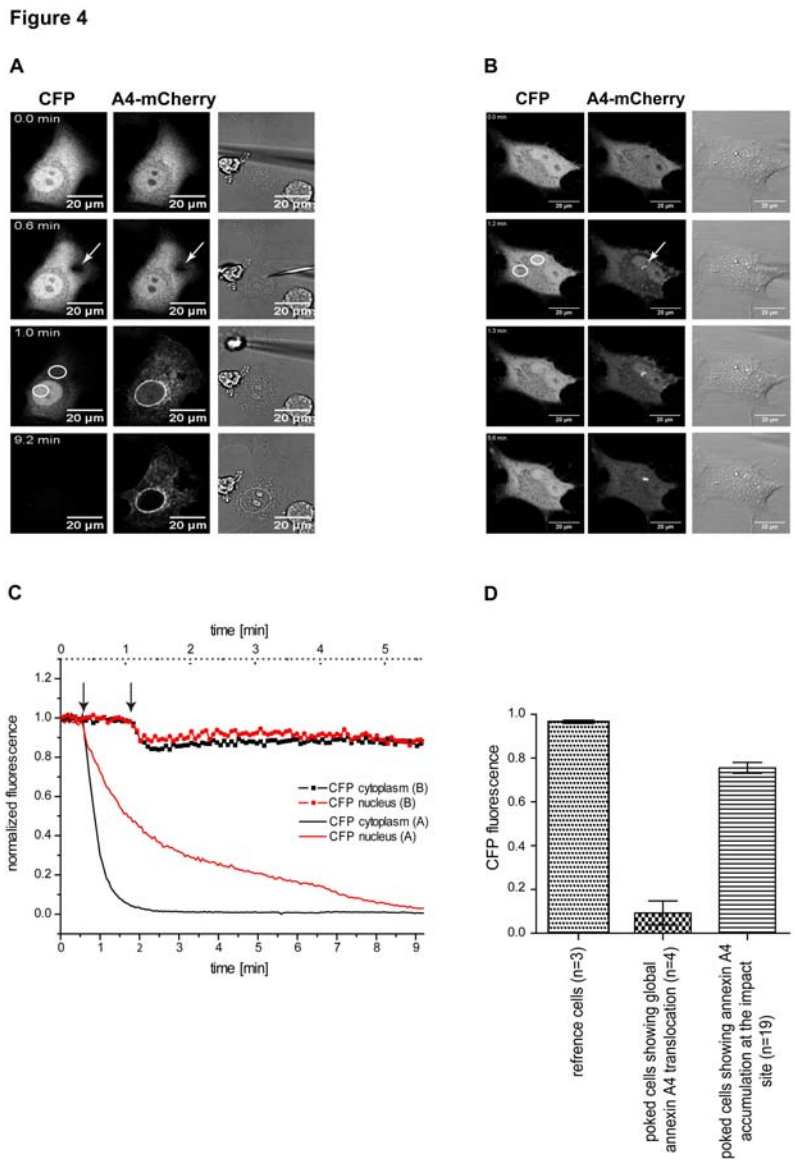

Figure 4. Prevention of CFP leakage correlates with proper annexin A4 accumulation at the impact site. (A) Microneedle puncturing induced a global translocation of annexin A4-mCherry to the nuclear envelope and to the plasma membrane. A dramatic loss in CFP fluorescence was observed. (B) Local accumulation of A4-mCherry maintained 80-90% of the initial CFP fluorescence over the image acquisition time after wounding the cell mechanically. Circles in A and B are indicating

regions used for image analysis shown in C. Arrows are indicating the position and time point of poking. (C) Traces of CFP expressing cell shown in A and B. (D) Statistical analysis of maintained CFP fluorescence after microneedle puncturing. Error bars are representing the SD.

High resolution imaging of impact sites by correlative fluorescence and electron microscopy combined with pre-embeddding immunogold labelling revealed the localization of annexin A4 – It was previously shown that the rapid accumulation of vesicles is instrumental for mending a membrane lesion (McNeil et al., 2000). In order to investigate the precise location of annexin A4 within the impact site in greater detail, we turned to correlative microscopy. Before the experiments, cover slips marked with a pulsed laser or commercially available gridded cell culture dishes were used to define the experimental area. Subsequently, cells located within this area were wounded with a glass needle and simultaneously imaged by laser scanning confocal microscopy (Colombelli et al., 2008; Sun et al., 1995). After a defined length of time (i.e. 3 min), the cells were fixed, immunolabeled, embedded and serial sectioned. Transmission electron microscopy micrographs were taken. The impact site after poking was here clearly visible as a hole with a diameter of 0.7 - 15 µm (Suppl. Figure S4 and Figure 5). Deeper slices showed a very dense and tightly packed structure (increased electron density) around the lesion. These dense structures often extended more than 500 nm into the cell body (Suppl. Figure S5 C-E). It still has to be clarified, if this dense structure reflects membrane structures as a result of vesicular ´patch´ formation or a dense contractile array formed by cytoskeletal

components like actin filaments or myosin (actomyosin) similar to those observed around wounds in *Xenopus* oocytes (Mandato and Bement, 2001).

The subcellular localization of annexin A4 was identified by pre-embedding immunogold EM. Annexin A4 N-terminally fused to GFP was expressed in HeLa cells. Cells were wounded mechanically by microneedle puncturing and immunogold labeling was performed against the GFP fusion protein to prevent crosstalk with the endogenous expressed annexin A4 or other endogenous expressed annexin subtypes. Due to the fact that the pre-embedding labeling procedure was used, which means applying the antibody directly to wounded cells after a slight fixation while growing on a cover slip, only regions in the cell which are accessible for the antibody are labeled.

Strong labeling was found at the border of the impact site (Suppl. Figure S5 B and C) as well as on aggregated vesicles (Figure 5E). This correlates with the position of the impact observed by fluorescence microscopy and supports the hypothesis that the annexin A4 array is the essential component to glue vesicles into one tight patch that prevents further calcium influx.

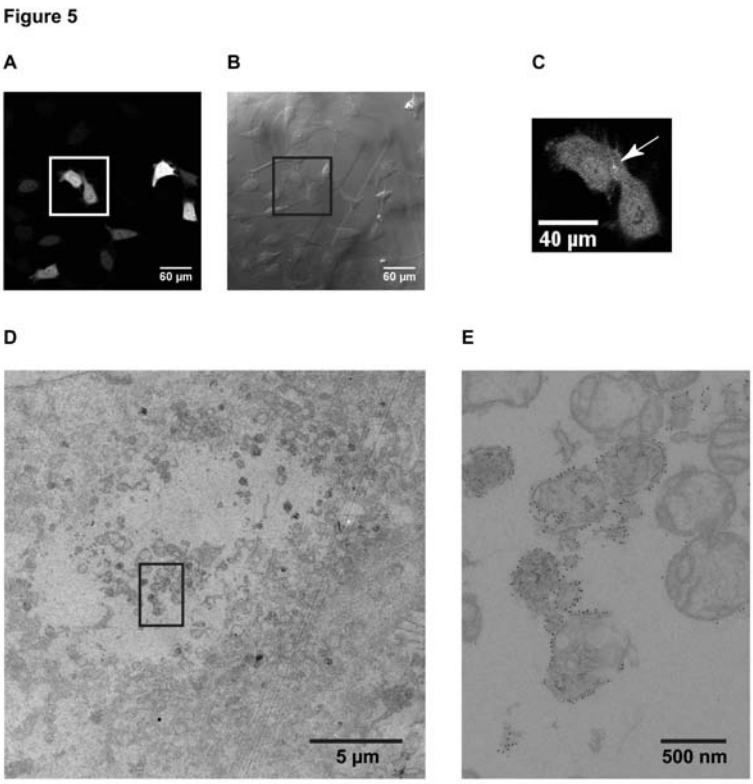

Figure 5. Immunogold electron microscopy revealed vesicular location of annexin A4. (A and B) Confocal fluorescence and transmission images of the experimental area. Rectangular regions in A and B are showing the cell of interest. (C) After microneedle puncturing, the translocation of GFP-annexin A4 to the impact was visible (indicated by an arrow). (D) In the overview electron micrograph the impact hole with a large number of small vesicles in the cavity was observed. (E) Immunogold labelling against the GFP fusion part of the annexin A4 revealed the vesicular location of annexin A4. Most of the gold particles were localized on the surface of the aggregating vesicles as well as at the rim of the impact site (Suppl. Figure S6).

Live-cell multiparameter imaging experiments unravel the timing of distinct signaling events induced by cellular wounding – Annexin A4 is only one of many proteins that bind phospholipids in a calcium-dependent way. Other proteins include the cysteine protease calpain, synaptotagmin VII as well as various isoforms of protein kinase C (PKC). All these proteins have been reported to be essential for membrane resealing (Chakrabarti et al., 2003; Mellgren et al., 2007; Reddy et al., 2001; Togo et al., 1999; Togo et al., 2000). Accordingly, we found that the GFP fusion protein of the calpain II large subunit readily translocated to the impact site (Suppl. Figure S6 A) after microneedle puncturing. Synaptotagmin VII-YFP, (Suppl. Figure S6 B) showed, different from annexin A4, mainly a global non-reversible plasma membrane translocation.

Annexin A4 is a substrate for PKC (Kaetzel et al., 2001; Weber et al., 1987). In addition, the resealing rate of membrane lesions is supressed in the presence of the PKC inhibitors Gö6976 and bisindolylmaleimide (BIS) (Togo et al., 1999). Therefore, we investigated the effect of a massive calcium influx on such proteins. After membrane rupture, PKCα C-terminally fused to GFP translocated to the impact site, however, with a different time course than annexin A4. In multiparameter experiments with mKate-labeled annexin A4 and GFP-fused PKCα, the significant difference in timing became obvious (Figure 6, Suppl. Movie 3). In fact, initially the calcium-sensitive PKCα translocated globally to the plasma membrane. After cytosolic calcium returned to normal, the PKC fusion left the plasma membrane and a fraction accumulated at the impact site 1.5-2 min after annexin A4 translocation. The non-classical PKC isoforms δ and ξ failed to translocate under these conditions (data not shown).

PKC isoforms are recruited to membranes either through elevated calcium levels sensed by the C2 domain or by binding to diacylglycerol (DAG) via the C1 domain or by both. Since calcium levels were already back to normal when PKCs started to translocate to the impact site, we investigated whether the translocation could be triggered by increased DAG levels in the 'patch'. We therefore expressed the C1-domain of PKCγ fused C-terminally to GFP either in combination with annexin A4-mCherry or with PKCα-mCherry. Similar to the PKCα-mCherry translocation behaviour the C1-domain showed at first a global plasma membrane translocation before accumulating at the impact site 1.5 -2 min after microneedle puncture (Figure 6 C and D). This indicated that DAG levels in the vesicular membrane system of the repair machinery were significantly elevated. It remains to be established whether these elevated DAG levels are due to an increased enzymatic activity of phospholipase C or phospholipase D (PLD) or due to diffusion of DAG molecules from membrane areas in the proximity of the lesion.

Figure 6

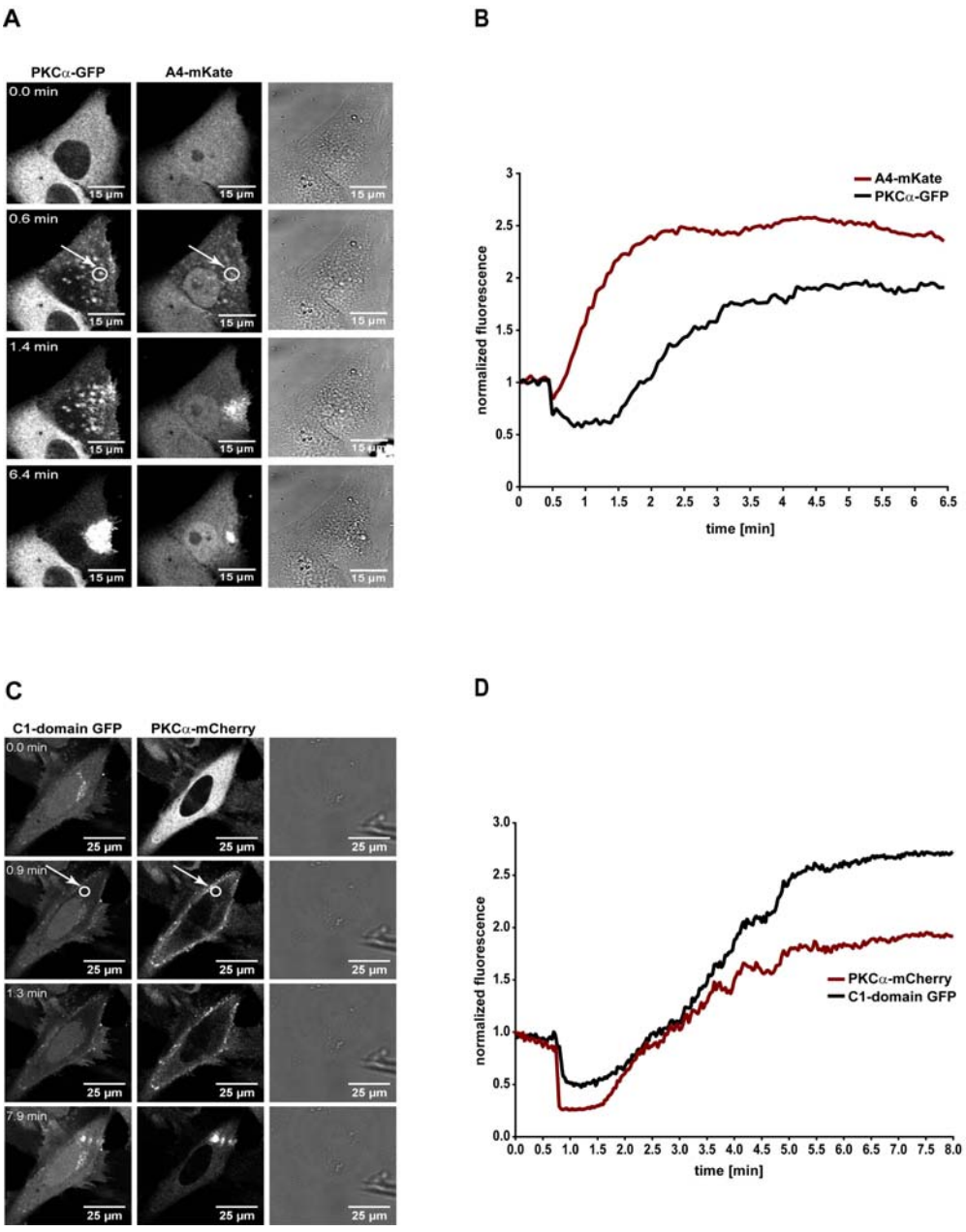

Figure 6. (A) Translocation behavior of PKCα–GFP in comparison to annexin A4-mKate after microneedle puncturing. Time series images of HeLa cells overexpressing PKCα-GFP and annexin A4-mKate are shown. Arrows in (A) indicate the impact site. Circles in (A) indicate the regions of interest used for data analysis in B. (B) Traces of

PKCα-GFP and annexin A4-mKate expressing cell shown in A. Data are representative of results obtained in 10 additional cells from 3 independent experiments. (C) Simultaneous measurements of PKCα–GFP translocation and DAG concentration at the impact site after membrane damage. Time series images of HeLa cells overexpressing PKCα-mCherry and C1-domain fused to GFP. Arrows in (C) indicate the impact site. Circles in (C) indicate the regions of interest used for data analysis in D. (D) Traces of PKCα-mCherry and C1-domain-GFP expressing cell shown in C. Data are representative of results obtained in 8 additional cells from 3 independent experiments.

DISCUSSION

Function of annexin A4 in membrane repair **-** Previously, the group of McNeil demonstrated that annexin A1 is important in cell membrane repair. Here we show by multiparameter imaging approaches, that the Ca^{2+} influx through the membrane lesion induces a fast and locally limited accumulation of annexin A4 to the impact site within less than 20 sec. This very early response of annexin A4 in comparison to other annexins used in our study indicates that annexin A4 is a primary target molecule in response to local calcium levels above several μM and that it acts as a very sensitive damage sensor for the repair machinery. The high FRET signal at the impact site observed in our study arises from high concentrations of annexin A4 molecules in this region and demonstrates the physiological role of annexin A4 self-association. This supports previous proposals by (Kaetzel et al., 2001) and (Zaks and Creutz, 1991), that annexin self-association may take place during membrane fusion or vesicle-vesicle aggregation - common events in the initial plasma membrane resealing steps after damaging (McNeil et al., 2000).

In addition, the postulated model by Kaetzel and co-workers (Kaetzel et al., 2001), where a well-ordered annexin A4 monolayer at the surface of liposomes mediated the fusion with other liposomes by interacting face-to-face with each other when coming into close proximity, shows strong similarities to our observations concerning the subcellular localization of annexin A4 by electron microscopy after mechanical wounding. Here, annexin A4 molecules are extensively coating the surface of vesicles located in the region of the impact as well as at the edge of the impact site. We conclude that our TEM micrographs illustrate an early step of the sealing procedure following the patch

hypothesis, where single vesicle-vesicle fusion events occur to form enlarged vesicles. This results in the formation of a patch which is eventually connecting to the plasma membrane. In all of these fusion and aggregation steps a role of annexin A4 in promoting or mediating these kinds of processes is plausible. In addition, annexin A4 may form an irreversible and rigid self-assembled monolayer at the cytoplasmic site of the patch even after the patch has connected to the plasma membrane in order to support the still fragile structure as well as to act as a scaffold protein for further vesicle recruitment or for proteins involved in the repair machinery (Figure 7, upper and middle illustration).

Individual functions of various annexins in membrane repair - Our results suggest that each of the annexins has different tasks in the repair process, orchestrated by a precise recruitment in space and time. It is unlikely that one annexin serves as a template for the formation of heterogeneous annexin assemblies, because previous studies in living cells showed no FRET between assemblies in the same area (Skrahina et al., 2008). Instead our results support the hypothesis that some annexins (A1, A2, A4, A6 and A7) recognize different defined membrane regions potentially characterized by a particular lipid composition. In addition, annexin A2 with its higher calcium affinity supports membranes in some distance to the impact site potentially to prevent further tearing of the damaged membrane. Interestingly, annexin A2 interacts with cell division cycle 42 (CDC42) (Martin-Belmonte et al., 2007), a small GTPase which accumulates in similar concentric assemblies around wounds in *Xenopus* oocytes (Benink and Bement, 2005) in a Ca^{2+}-dependent manner. Since CDC42 has key functions in regulating actin

cytoskeleton dynamics and annexin A2 is known to act as a linker between the plasma membrane and the cytoskeleton both proteins might be instrumental in reforging the actin cytoskeleton at the end of the repair process. It appears that several of the annexins help in membrane repair in a slightly different fashion, either to serve cell-type specific needs or because only concerted activities of many phospholipid-binding proteins will help in the threat of membrane damage.

Annexins as scaffolds for signaling molecules - Other annexin isoforms such as A1 and A6 seem to add layers of aggregates later in the process. At the same time, about two minutes after impact, proteins relevant in intracellular signaling such as some of the PKC isoforms are recruited. Many of the annexins such as A1, A4, A5 and A6 are known interaction partners of protein kinase C isoforms (Schmitz-Peiffer et al., 1998), even e.g. as substrates (A1, A2, A4) or as inhibitors (A5). Since inhibition of PKC decreases the resealing rate of a membrane lesion significantly (Togo et al., 1999) it is no too far-fetched that the interaction of annexins with PKC is instrumental for membrane repair. Although the interaction of annexin A4 and PKCα could not be demonstrated by FRET (data not shown), it does not exclude a more transient interaction such as a protein-substrate interaction. Our imaging results show that the initial global attachment of PKCα to the plasma membrane, due to the strong calcium influx, prevents PKC leakage through the lesion. On the other hand, it is also a possible mechanism to prevent the proteolytic degradation of PKC by calpain II, which is only active at very high calcium concentrations (mM range) but located at the impact site as well (Mikawa, 1990). After

the calcium influx is stopped by annexin A4-mediated vesicle fusion at the impact site, PKCα as well as signaling-relevant lipids such as DAG are transiently accumulating in the region of the lesion with some delay in timing. Since the phosphorylation of annexin A4 by PKCα inhibits annexin A4 mediated vesicle-vesicle fusion events *in vitro* (Kaetzel et al., 2001), it can be speculated that the delay of PKCα translocation in the repair process is part of the termination signal to stop further vesicle – vesicle fusion events at the impact site or further vesicle recruitment. In addition, PKCα, already located at the membrane lesion, can regulate very locally other signaling molecules relevant in membrane repair or membrane/cytoskeleton remodeling (Figure 7, bottom illustration). The accumulation of DAG suggests that the impact site may be equipped with a special subset of lipids that attracts the signaling machinery required for repairing the lesion. DAG, crucial for PKC activity, may protect the proteolytic cleavage of PKC by calpain II (Lang et al., 1995). All single translocation and biosynthesis steps might be part of a tightly timed program and the formation of scaffold-like protein-lipid complexes initiated by the calcium influx from the membrane lesion. This indicates that cells are well-prepared to deal with physical impact and that membrane repair is a standard procedure in the physiology of the cell.

Figure 7

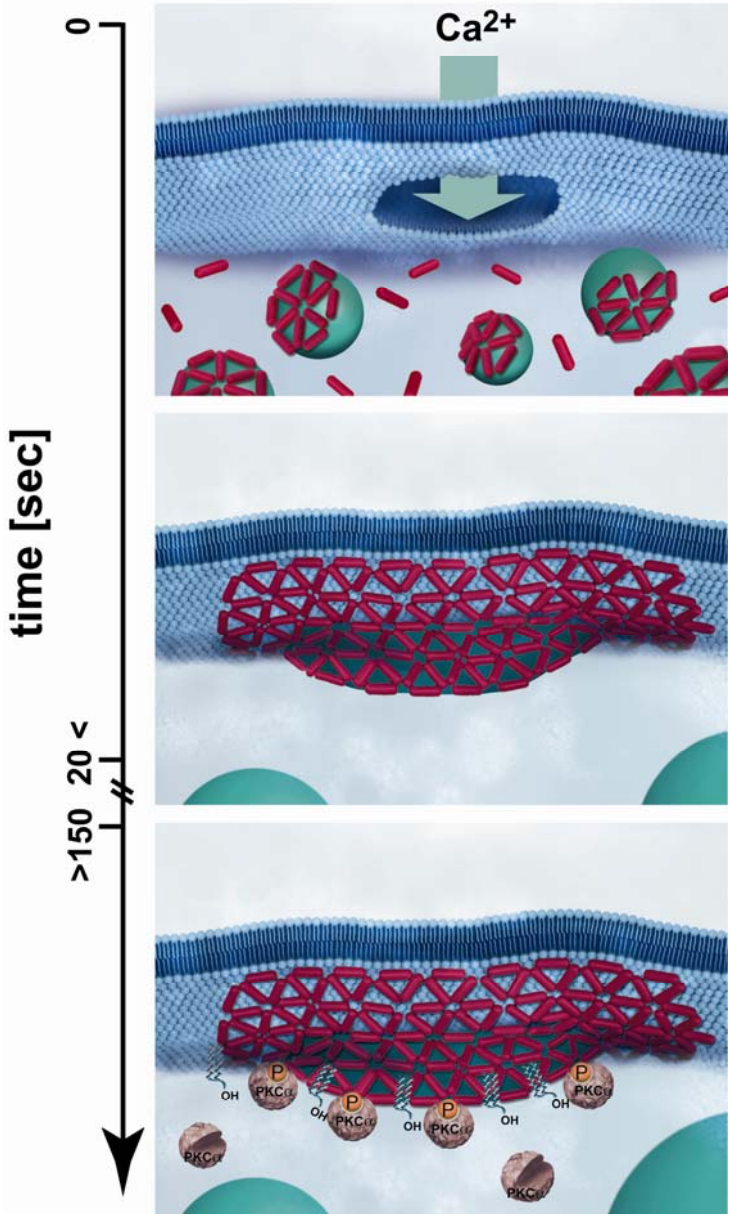

Figure 7: Hypothesized model of annexin A4 function in plasma membrane repair. The upper illustration shows the Ca^{2+}-influx through a membrane lesion, activating and triggering vesicle-vesicle fusion events for resealing the membrane. Beside the cytoplasmatic annexin A4 fraction (red rods), some annexin A4 molecules are located, probably prearranged on vesicles (green spheres), as shown by EM. A mechanical support of the patch becomes obvious, when looking at the highly ordered annexin A4

monolayer as a result of annexin A4 self-association (middle illustration). CYNEX measurements as well as TFP experiments are supporting that the annexinA4 self-association event at the lesion is cruical. With a time delay of 1.5-2 min PKCα as well as DAG are increased at the impact site (bottom illustration), making a function of this monolayer as a scaffold plausible. Here, PKCα mediated annexin A4 phosphorylation can e.g. lead to terminate further vesicle recruitment or further to trigger very locally signaling pathways necessary for membrane repair or membrane/cytoskeleton remodeling.

Conclusion and Outlook – Plasma membrane ruptures are easily repaired unless a certain size of the lesion is exceeded. The mending is strictly local although initially a strong but short calcium influx affects the entire cell. Due to this local and transient nature and the similarity of the calcium transient to receptor-induced changes in intracellular calcium levels, it is very difficult to study membrane repair by standard biochemistry. Therefore, imaging of fluorescently tagged proteins and its correlation with electron micrographs is an appropriate way to identify spatio-temporal relationships of molecular components in the repair process. In this study, we used fluorescent fusion proteins and fluorescence live cell imaging techniques to visualize translocation phenomena of plasma membrane repair in real-time. The study establishes annexins as pivotal components to rapidly seal the plasma membrane after physical impact. The lead role and the precise location of annexin A4 in this process was demonstrated by correlative fluorescence and immuno-electron microscopy. The results indicated that annexin A4 acts in the repair machinery as an early

damage sensor for recognizing membrane ruptures as well as a scaffold molecule to assemble vesicles in the patch formation. The identification and visualization of signaling molecules such as PKC and DAG suggests that after membrane rupture a precisely timed molecular repair machinery is involved for reinstalling membrane integrity. Imaging of more signaling components in a time-resolved manner is required to deliver a more complete picture of the signaling network and to link it to the various stages of the repair process including vesicle to membrane fusion and the repair of the actin cytoskeleton. This will lead to the identification of drugable target molecules mediating or preventing membrane repair and ultimating the treatment of muscle dystrophies and associated cardiomyopathies.

MATERIALS AND METHODS

Cloning – Cloning of different C-terminal fluorescent fusion proteins of various human annexins is described elsewhere (Piljic and Schultz, 2006; Skrahina et al., 2008). Cloning of annexin A 4 C-terminal fused to mCherry is described in (Piljic and Schultz, 2008). Annexin A4-mKate was generated by subcloning. The coding sequence of annexin A4 from pECFP-N1-annexin A4 (Piljic and Schultz, 2006) was excised and ligated into mKate-N1 (Evrogen, Russia). Cloning of the pEYFP-N1 annexin A9 construct was performed by PCR amplification of human annexin A9 cDNA (RZPD, IRAUp969G0626D6, BC005830). 5' EcoRI and 3' BamHI restriction sites were inserted and the PCR-product ligated in pEYFP-N1 (Clontech, Germany) linerazied accordingly. Mutations in the annexin A4 coding sequence were generated via the QuikChange® site-directed mutagenesis kit (Stratagene, USA), according to the manufacturer's guidelines. mEGFP-annexin A4 fusion construct as well as the mPlum-annexin A4 fusion construct was a kind gift of Michael W. Davidson (NHMFL, Tallahassee, Florida, USA). Cloning of the annexin A4 based FRET sensor CYNEX4 (EYFP-annexin A4-ECFP) is described in (Piljic and Schultz, 2006). Construction of the human PKCα C-terminally fused to GFP is described by (Reither et al., 2006). PKCα-mCherry was generated accordingly. Both constructs were kindly provided by Gregor Reither. The C1-domain of PKCγ C-terminally fused to GFP was a kind gift of Tobias Meyer (Stanford University Medical Center, Stanford, California, USA). Standard PCR and cloning techniques were used to introduce a 5' Hind III and 3' Sal1 restriction site into the coding sequence of human

synaptotagmin VII (origene, USA, NM_004200) and the human large subunit of Calpain II (m-Calpain, origene, USA, NM_001748). PCR products were ligated after double-digestion with HindIII and Sal1 into pEGFP-C1 (Calpain II) or pEYFP-N1 (SynVII) (Clontech, Germany), linearized accordingly. In case of pEYFP-N1 Synaptotagmin VII the removing of the stop codon of the synaptotagmin VII cDNA was performed in the PCR step additionally. All constructs were verified by DNA sequencing.

Cell culture and transfection – HeLa (ATCC CCL-2) were cultured in Dulbecco's modified Eagle's medium supplemented with 10% fetal bovine serum (Gibco-BRL) and 0.1 mg/ml primocin (InvivoGen, San Diego, California, USA) at 37°C in a humidified atmosphere of air and 5% CO_2. For imaging experiments, cells were seeded in 35-mm glas bottom MatTek dishes (MatTek Corp., Ashland, MA, USA) and transfected at 50-70% confluency. For correlative fluorescence and electron microscopy cells were seeded in 35- mm gridded or laser marked glas bottom MatTek dishes. HeLa cells were transiently transfected with plasmid-DNA using FuGENE 6 reagent (Roche, Mannheim, Germany). Transfections were performed in Opti-MEM (Invitrogen, Karlsruhe, Germany) according to manufacturer's instructions. For microscopy, cells were washed 16-48 h after transfection and growth medium was replaced with pre-warmed imaging buffer (20 mM HEPES, pH 7.4, 115 mM NaCl, 1.2 mM $CaCl_2$, 1.2 mM $MgCl_2$, 1.2 mM K_2HPO_4, 2 g/l D-glucose).

Confocal microscopy and image analysis – Time series of annexin translocation after mechanical cellular wounding (poking) were recorded on a confocal Leica TCS SP2 AOBS microscope (Leica Microsystems, Mannheim, Germany) equipped with an Eppendorf micromanipulator (Eppendorf, Hamburg, Germany) using a HCX PL APO CS 40.0 × 1.25 oil or a HCX PL APO lbd.BL. 63.0 x 1.40 oil objective at room temperature. Image acquisition was performed using Leica LCS Image software (version 2.5, Leica Microsystems, Mannheim, Germany). Laser power and PMT gain were adjusted individually for each experiment. Images were taken in 8-bit mode with 0.815 – 3.714 s between frames. The following fluorescence excitation and emission settings were used: ECFP (ex. 405 nm, em. 450–480 nm), Fluo-4 and EGFP (ex. 488 nm, em. 495–520 nm), mCherry (ex. 594 nm, em. 640-700 nm), mKate and mPlum (ex. 594 nm, em. 640–750 nm). For calcium-imaging experiments cells were incubated with 5 μM Fluo-4/AM (Molecular Probes, Invitrogen, Karlsruhe, Germany) for 30 min at room temperature. Cells were washed with PBS and incubated in fresh imaging medium. CYNEX measurements and FRET efficiency calculation were performed as described in Piljic and Schultz, 2006.Microinjection needles (filamented borosilicate glass capillaries GC120 TF-10, 1.2 mm outer diameter and 0.94 mm inner diameter; Harvard Apparatus Ltd, Edenbridge, Kent, UK) were pulled by a conventional air-jet puller (P97, Sutter Instruments, Novato, CA, USA). Micropipette puller settings were heat = 520, pull = 100, velocity = 100, time = 120. The average needle tip diameter was around 0.3 μm.

For laser nanosurgery an Olympus FluoView1000 equipped with a 375 nm pulsed laser diode (LDH-D 375, PicoQuant, Berlin, Germany) was used. A 60x 1.2 NA water (UIS2) Image acquisition was performed using Olympus FV10-ASW software (version

01.07.02.02, Olympus). For ionomycin experiments, the compound (Calbiochem, Germany) was dissolved in DMSO before adding it to cells to a final concentration of 5 μM. Trifluorperazine hydrochloride (Fluka, Germany) was dissolved in water.

Images were processed and analyzed using Image J software (Rasband, W.S., ImageJ, U.S. National Institutes of Health, Bethesda, Maryland, USA). All images were background corrected and smoothed with a median filter (0.5). In some cases the contrast was enhanced for better visualization. Data sets of the ROI fluorescence over time were transferred into Origin software (version 8; OriginLab Corporation, Northampton, Massachusetts, USA) for data visualization.

Pre-embedding immunogold labelling / electron microscopy - Immunogold labelling of the wounded HeLa cells growing in a monolayer on MatTek dishes with a gridded cover slip was followed by flat-embedding in EPON. For the labelling procedure cells were prefixed for 10 min at room temperature in 4% paraformaldehyde, 0.1% glutaraldehyde in100mM phosphate buffer supplemented with 2% sucrose. The cells were then rinsed with 100 mM phosphate buffer and the aldehydes were quenched by 10 min incubation in 50 mM glycin in PBS. The cells were subsequently blocked in 5% FCS in PBS for 20 min. Blocking was followed by 20 min incubation in primary antibody, goat anti-GFP 1:70 (Rockland Immunochemicals), and 20 min incubation in the linker antibody rabbit anti goat 1:150 (Dako, Denmark). Finally, the cells were incubated for 20 min in colloidal gold conjugated protein A, 10 nm gold particle size, 1:75 (CMC University medical center Utrecht, Nederlands). Antibodies and protein A-Gold were diluted in blocking

buffer. Between each antibody incubation step, the sample was rinsed with PBS. The samples were then prepared for flat-embedding. Cells were fixed in 2.5 % glutaraldehyde in 50 mM CaCodylate buffer supplemented with 2 % sucrose, 50mM KCl, 2.6mM $CaCl_2$ and 2.6mM $MgCl_2$ for 30 min at room temperature and rinsed in cacodylate buffer. The following procedure was then performed on ice. First, samples were incubated in 1% osmium in cacodylate buffer for 40 min, rinsed in water and incubated in 0.5% uranylacetate in water for 30 min. The contrast enhancement steps were followed by a stepwise dehydration in ethanol, up to 100% ethanol and a final dip of the cover slips in propylene oxide before they were placed on EPON (Roth, Germany) filled beam capsules for flat embedding. Polymerization was done at 60°C. The position of the wounded cells was identified by the marks from the grid pattern on the cover slip, which are imprinted on the EPON blocks. The defined area was trimmed and sectioned in ultrathin sections (60-70 nm thickness) by an ultramicrotome (Leica Microsystems,Vienna, Austria). Serial sections were mounted on formvar coated slot grids, and contrasted with uranyl acetate and lead citrate. The sections were then viewed and pictures were acquired in a CM120 biotwin electron microscope (FEI, Eindoven, The Netherlands) operating at 100 kV. Digital acquisitions were made with a Keen View CCD camera (Soft Imaging System, Muenster, Germany). The wounded cells were identified by comparing the cell patterns from fluorescence microscopy images taken at the time of poking, with the cell pattern in the section.

ACKNOWLEDGMENTS

We would like to thank Stefan Terjung of EMBL's Advanced Light Microscopy Facility, Tatsiana Skrahina for generating pEYFP-N1 annexin A9 and Heike Stichnoth for cultured cells. We thank Vibor Laketa and Jan Ellenberg for critical reading the manuscript. This work was supported in part by a grant from the EU (LSHG-CT-2003-503259 to C.S.).

ABBREVIATIONS

A1-GFP, annexin A1-GFP; A2-CFP, annexin A2-CFP, A4-mCherry, annexin A4-mCherry; A4-mKate, annexin A4-mKate; A5-GFP, annexin A5-GFP; A6-CFP, annexin A6-CFP; A7-GFP, annexin A7-GFP; AOBS, Acousto-Optical Beam Splitter; $[Ca^{2+}]_i$, intracellular calcium concentration; CYNEX4, cyan-yellow-labeled annexin A4; ECFP, enhanced cyan fluorescent protein; EYFP, enhanced yellow fluorescent protein; EM, electron microscopy; FRET, fluorescence resonance energy transfer; mPlum-A4, mPlum-annexin A4; SynVII-YFP, Synaptotagmin VII-YFP, TEM, transmission electron microscopy; TFP, Trifluorperazine.

REFERENCES

Babbin, B.A., M.G. Laukoetter, P. Nava, S. Koch, W.Y. Lee, C.T. Capaldo, E. Peatman, E.A. Severson, R.J. Flower, M. Perretti, C.A. Parkos, and A. Nusrat. 2008. Annexin A1 regulates intestinal mucosal injury, inflammation, and repair. *J Immunol*. 181:5035-44.

Babbin, B.A., C.A. Parkos, K.J. Mandell, L.M. Winfree, O. Laur, A.I. Ivanov, and A. Nusrat. 2007. Annexin 2 regulates intestinal epithelial cell spreading and wound closure through Rho-related signaling. *Am J Pathol*. 170:951-66.

Bansal, D., and K.P. Campbell. 2004. Dysferlin and the plasma membrane repair in muscular dystrophy. *Trends Cell Biol*. 14:206-13.

Bansal, D., K. Miyake, S.S. Vogel, S. Groh, C.C. Chen, R. Williamson, P.L. McNeil, and K.P. Campbell. 2003. Defective membrane repair in dysferlin-deficient muscular dystrophy. *Nature*. 423:168-72.

Barwise, J.L., and J.H. Walker. 1996. Annexins II, IV, V and VI relocate in response to rises in intracellular calcium in human foreskin fibroblasts. *J Cell Sci*. 109 (Pt 1):247-55.

Bement, W.M., H.Y. Yu, B.M. Burkel, E.M. Vaughan, and A.G. Clark. 2007. Rehabilitation and the single cell. *Curr Opin Cell Biol*. 19:95-100.

Benink, H.A., and W.M. Bement. 2005. Concentric zones of active RhoA and Cdc42 around single cell wounds. *J Cell Biol*. 168:429-39.

Blackwood, R.A., and J.D. Ernst. 1990. Characterization of Ca2(+)-dependent phospholipid binding, vesicle aggregation and membrane fusion by annexins. *Biochem J*. 266:195-200.

Cagliani, R., F. Magri, A. Toscano, L. Merlini, F. Fortunato, C. Lamperti, C. Rodolico, A. Prelle, M. Sironi, M. Aguennouz, P. Ciscato, A. Uncini, M. Moggio, N. Bresolin, and G.P. Comi. 2005. Mutation finding in patients with dysferlin deficiency and role of the dysferlin interacting proteins annexin A1 and A2 in muscular dystrophies. *Hum Mutat*. 26:283.

Chakrabarti, S., K.S. Kobayashi, R.A. Flavell, C.B. Marks, K. Miyake, D.R. Liston, K.T. Fowler, F.S. Gorelick, and N.W. Andrews. 2003. Impaired membrane resealing and autoimmune myositis in synaptotagmin VII-deficient mice. *J Cell Biol*. 162:543-9.

Clarke, M.S., R.W. Caldwell, H. Chiao, K. Miyake, and P.L. McNeil. 1995. Contraction-induced cell wounding and release of fibroblast growth factor in heart. *Circ Res*. 76:927-34.

Colombelli, J., C. Tangemo, U. Haselman, C. Antony, E.H. Stelzer, R. Pepperkok, and E.G. Reynaud. 2008. A correlative light and electron microscopy method based on laser micropatterning and etching. *Methods Mol Biol*. 457:203-13.

Dreier, R., K.W. Schmid, V. Gerke, and K. Riehemann. 1998. Differential expression of annexins I, II and IV in human tissues: an immunohistochemical study. *Histochem Cell Biol*. 110:137-48.

Filipenko, N.R., H.M. Kang, and D.M. Waisman. 2000. Characterization of the Ca2+-binding sites of annexin II tetramer. *J Biol Chem*. 275:38877-84.

Gerke, V., and S.E. Moss. 1997. Annexins and membrane dynamics. *Biochim Biophys Acta*. 1357:129-54.

Glenney, J. 1986. Phospholipid-dependent Ca2+ binding by the 36-kDa tyrosine kinase substrate (calpactin) and its 33-kDa core. *J Biol Chem*. 261:7247-52.

Goulet, F., K.G. Moore, and A.C. Sartorelli. 1992. Glycosylation of annexin I and annexin II. *Biochem Biophys Res Commun*. 188:554-8.

Han, R., D. Bansal, K. Miyake, V.P. Muniz, R.M. Weiss, P.L. McNeil, and K.P. Campbell. 2007. Dysferlin-mediated membrane repair protects the heart from stress-induced left ventricular injury. *J Clin Invest*. 117:1805-13.

Janshoff, A., M. Ross, V. Gerke, and C. Steinem. 2001. Visualization of annexin I binding to calcium-induced phosphatidylserine domains. *Chembiochem*. 2:587-90.

Jost, M., C. Thiel, K. Weber, and V. Gerke. 1992. Mapping of three unique Ca(2+)-binding sites in human annexin II. *Eur J Biochem*. 207:923-30.

Kaetzel, M.A., P. Hazarika, and J.R. Dedman. 1989. Differential tissue expression of three 35-kDa annexin calcium-dependent phospholipid-binding proteins. *J Biol Chem*. 264:14463-70.

Kaetzel, M.A., P. Hazarika, M. Diaz-Munoz, W. Dubinsky, S.L. Hamilton, and J.R. Dedman. 1990. Annexins: a subcellular localization and reconstitution approach to elucidate cellular function. *Biochem Soc Trans*. 18:1108-10.

Kaetzel, M.A., Y.D. Mo, T.R. Mealy, B. Campos, W. Bergsma-Schutter, A. Brisson, J.R. Dedman, and B.A. Seaton. 2001. Phosphorylation mutants elucidate the mechanism of annexin IV-mediated membrane aggregation. *Biochemistry*. 40:4192-9.

Kaetzel, M.A., G. Pula, B. Campos, P. Uhrin, N. Horseman, and J.R. Dedman. 1994. Annexin VI isoforms are differentially expressed in mammalian tissues. *Biochim Biophys Acta*. 1223:368-74.

Kohli, V., A.Y. Elezzabi, and J.P. Acker. 2005. Cell nanosurgery using ultrashort (femtosecond) laser pulses: applications to membrane surgery and cell isolation. *Lasers Surg Med*. 37:227-30.

Kubista, H., S. Sacre, and S.E. Moss. 2000. Annexins and membrane fusion. *Subcell Biochem*. 34:73-131.

Lammerding, J., and R.T. Lee. 2007. Torn apart: membrane rupture in muscular dystrophies and associated cardiomyopathies. *J Clin Invest*. 117:1749-52.

Lang, D., M.L. Beermann, G. Hauser, C.M. Cressman, and T.B. Shea. 1995. Phospholipids inhibit proteolysis of protein kinase C alpha by mM calcium-requiring calpain. *Neurochem Res*. 20:1361-4.

Lemasters, J.J., J. DiGuiseppi, A.L. Nieminen, and B. Herman. 1987. Blebbing, free Ca2+ and mitochondrial membrane potential preceding cell death in hepatocytes. *Nature*. 325:78-81.

Lennon, N.J., A. Kho, B.J. Bacskai, S.L. Perlmutter, B.T. Hyman, and R.H. Brown, Jr. 2003. Dysferlin interacts with annexins A1 and A2 and mediates sarcolemmal wound-healing. *J Biol Chem*. 278:50466-73.

Luft, F.C. 2007. Dysferlin, dystrophy, and dilatative cardiomyopathy. *J Mol Med*. 85:1157-9.

Mandato, C.A., and W.M. Bement. 2001. Contraction and polymerization cooperate to assemble and close actomyosin rings around Xenopus oocyte wounds. *J Cell Biol*. 154:785-97.

Martin-Belmonte, F., A. Gassama, A. Datta, W. Yu, U. Rescher, V. Gerke, and K. Mostov. 2007. PTEN-mediated apical segregation of phosphoinositides controls epithelial morphogenesis through Cdc42. *Cell*. 128:383-97.

McNeil, A.K., U. Rescher, V. Gerke, and P.L. McNeil. 2006. Requirement for annexin A1 in plasma membrane repair. *J Biol Chem*. 281:35202-7.

McNeil, P.L. 2001. Direct introduction of molecules into cells. *Curr Protoc Cell Biol*. Chapter 20:Unit 20 1.

McNeil, P.L., and S. Ito. 1989. Gastrointestinal cell plasma membrane wounding and resealing in vivo. *Gastroenterology*. 96:1238-48.

McNeil, P.L., and R. Khakee. 1992. Disruptions of muscle fiber plasma membranes. Role in exercise-induced damage. *Am J Pathol*. 140:1097-109.

McNeil, P.L., and T. Kirchhausen. 2005. An emergency response team for membrane repair. *Nat Rev Mol Cell Biol*. 6:499-505.

McNeil, P.L., R.F. Murphy, F. Lanni, and D.L. Taylor. 1984. A method for incorporating macromolecules into adherent cells. *J Cell Biol*. 98:1556-64.

McNeil, P.L., L. Muthukrishnan, E. Warder, and P.A. D'Amore. 1989. Growth factors are released by mechanically wounded endothelial cells. *J Cell Biol*. 109:811-22.

McNeil, P.L., and M. Terasaki. 2001. Coping with the inevitable: how cells repair a torn surface membrane. *Nat Cell Biol*. 3:E124-9.

McNeil, P.L., S.S. Vogel, K. Miyake, and M. Terasaki. 2000. Patching plasma membrane disruptions with cytoplasmic membrane. *J Cell Sci*. 113 (Pt 11):1891-902.

McNeil, P.L., and E. Warder. 1987. Glass beads load macromolecules into living cells. *J Cell Sci*. 88 (Pt 5):669-78.

Mellgren, R.L., W. Zhang, K. Miyake, and P.L. McNeil. 2007. Calpain is required for the rapid, calcium-dependent repair of wounded plasma membrane. *J Biol Chem*. 282:2567-75.

Mikawa, K. 1990. Studies on proteolysis of protein kinase C with calpain I and II. *Kobe J Med Sci*. 36:55-69.

Miyake, K., P.L. McNeil, K. Suzuki, R. Tsunoda, and N. Sugai. 2001. An actin barrier to resealing. *J Cell Sci*. 114:3487-94.

Nelson, M.R., and C.E. Creutz. 1995. Combinatorial mutagenesis of the four domains of annexin IV: effects on chromaffin granule binding and aggregating activities. *Biochemistry*. 34:3121-32.

Orrenius, S., B. Zhivotovsky, and P. Nicotera. 2003. Regulation of cell death: the calcium-apoptosis link. *Nat Rev Mol Cell Biol*. 4:552-65.

Piljic, A., and C. Schultz. 2006. Annexin A4 self-association modulates general membrane protein mobility in living cells. *Mol Biol Cell*. 17:3318-28.

Piljic, A., and C. Schultz. 2008. Simultaneous recording of multiple cellular events by FRET. *ACS Chem Biol*. 3:156-60.

Raynal, P., and H.B. Pollard. 1994. Annexins: the problem of assessing the biological role for a gene family of multifunctional calcium- and phospholipid-binding proteins. *Biochim Biophys Acta*. 1197:63-93.

Reddy, A., E.V. Caler, and N.W. Andrews. 2001. Plasma membrane repair is mediated by Ca(2+)-regulated exocytosis of lysosomes. *Cell*. 106:157-69.

Reither, G., M. Schaefer, and P. Lipp. 2006. PKCalpha: a versatile key for decoding the cellular calcium toolkit. *J Cell Biol*. 174:521-33.

Rothhut, B. 1997. Participation of annexins in protein phosphorylation. *Cell Mol Life Sci*. 53:522-6.

Schmitz-Peiffer, C., C.L. Browne, J.H. Walker, and T.J. Biden. 1998. Activated protein kinase C alpha associates with annexin VI from skeletal muscle. *Biochem J*. 330 (Pt 2):675-81.

Schultz, C., A. Schleifenbaum, J. Goedhart, and T.W. Gadella, Jr. 2005. Multiparameter imaging for the analysis of intracellular signaling. *Chembiochem*. 6:1323-30.

Shen, S.S., and R.A. Steinhardt. 2005. The mechanisms of cell membrane resealing in rabbit corneal epithelial cells. *Curr Eye Res*. 30:543-54.

Shen, S.S., W.C. Tucker, E.R. Chapman, and R.A. Steinhardt. 2005. Molecular regulation of membrane resealing in 3T3 fibroblasts. *J Biol Chem*. 280:1652-60.

Skrahina, T., A. Piljic, and C. Schultz. 2008. Heterogeneity and timing of translocation and membrane-mediated assembly of different annexins. *Exp Cell Res*. 314:1039-47.

Steinhardt, R.A., G. Bi, and J.M. Alderton. 1994. Cell membrane resealing by a vesicular mechanism similar to neurotransmitter release. *Science*. 263:390-3.

Sun, X.J., L.P. Tolbert, and J.G. Hildebrand. 1995. Using laser scanning confocal microscopy as a guide for electron microscopic study: a simple method for correlation of light and electron microscopy. *J Histochem Cytochem*. 43:329-35.

Swanson, J.A., and P.L. McNeil. 1987. Nuclear reassembly excludes large macromolecules. *Science*. 238:548-50.

Terasaki, M., K. Miyake, and P.L. McNeil. 1997. Large plasma membrane disruptions are rapidly resealed by Ca2+-dependent vesicle-vesicle fusion events. *J Cell Biol*. 139:63-74.

Togo, T., J.M. Alderton, G.Q. Bi, and R.A. Steinhardt. 1999. The mechanism of facilitated cell membrane resealing. *J Cell Sci*. 112 (Pt 5):719-31.

Togo, T., J.M. Alderton, and R.A. Steinhardt. 2000. The mechanism of cell membrane repair. *Zygote*. 8 Suppl 1:S31-2.

Weber, K., N. Johnsson, U. Plessmann, P.N. Van, H.D. Soling, C. Ampe, and J. Vandekerckhove. 1987. The amino acid sequence of protein II and its phosphorylation site for protein kinase C; the domain structure Ca2+-modulated lipid binding proteins. *EMBO J*. 6:1599-604.

Wice, B.M., and J.I. Gordon. 1992. A strategy for isolation of cDNAs encoding proteins affecting human intestinal epithelial cell growth and differentiation: characterization of a novel gut-specific N-myristoylated annexin. *J Cell Biol*. 116:405-22.

Yu, Q.C., and P.L. McNeil. 1992. Transient disruptions of aortic endothelial cell plasma membranes. *Am J Pathol*. 141:1349-60.

Zaks, W.J., and C.E. Creutz. 1991. Ca(2+)-dependent annexin self-association on membrane surfaces. *Biochemistry*. 30:9607-15.

SUPPLEMENTAL MATERIAL

Figure S1. Simultaneous imaging of annexin A3, annexin A7, annexin A9 and annexin A4 translocation to the impact site after mechanical wounding. (A) Time series images of an annexin A3-CFP, annexin A7-GFP and mPlum-annexin A4 co-expressing HeLa cell were acquired simultaneously after wounding the cell with a glass needle. Arrows in A indicate the impact site. Circles in A indicate the region of interest used for data analysis in (B). (B) Translocation traces of annexin A3-CFP, annexin A7-GFP and mPlum-annexin A4 expressing cell shown in A. Again, in comparison to annexin A7 and annexin A3, annexin A4 is the fastest subtype arriving at the impact site. (C) Time series images of an annexin A9-YFP and annexin A4-mKate co-expressing HeLa cell were acquired simultaneously after microneedle puncturing. Arrows in C indicate the impact site. Circles in C indicate the region of interest used for data analysis in (D). (D) Translocation traces of annexin A9-YFP in comparison to annexin A4-mKate.

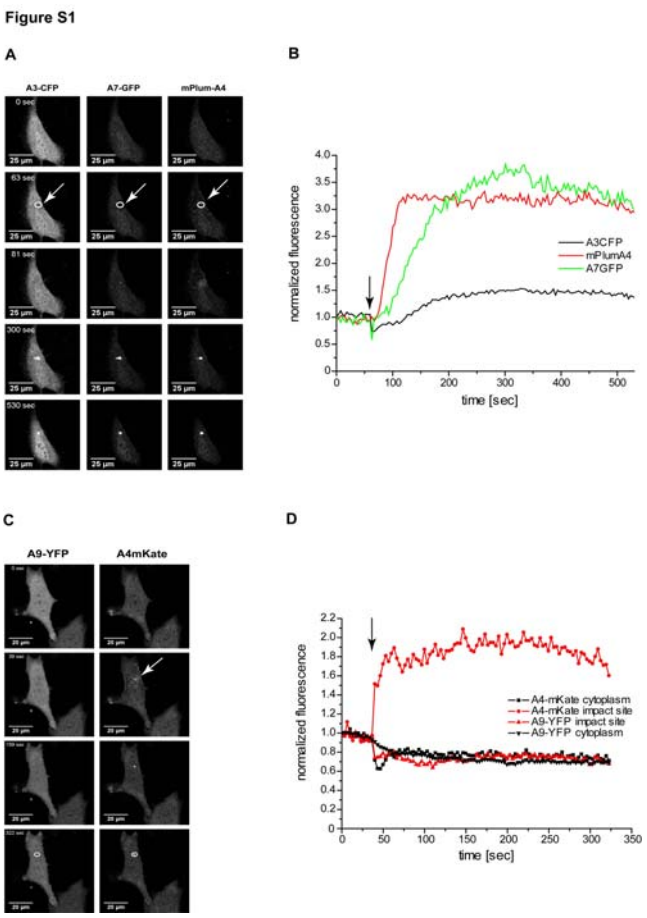

Figure S2. Laser nanosurgery of a HeLa cell expressing annexin A4-mCherry and loaded with Fluo-4 for visualizing Ca^{2+} entry. (A) A 5 sec treatment of the cell with a UV laser pulse (375nm) lead to a significant increase in the fluorescence intensity of Fluo-4 reflecting the Ca^{2+}-influx. A massiv and local accumulation of annexin A4-mCherry at the impact site was observed. Arrows are indicating the wounded area. The circle shows the region of interest used for data analysis (Fig. S1 B). (B) Traces of Fluo-4 response and annexin A4 translocation of the cell shown in (A).

A

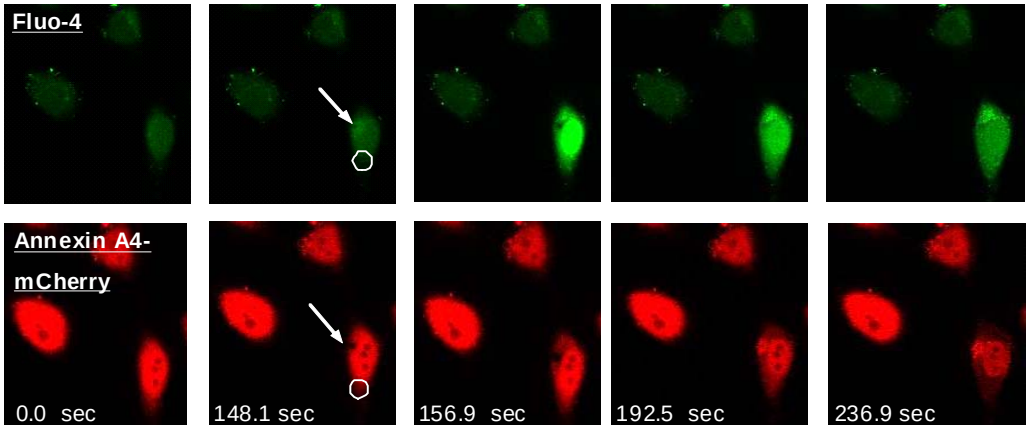

B

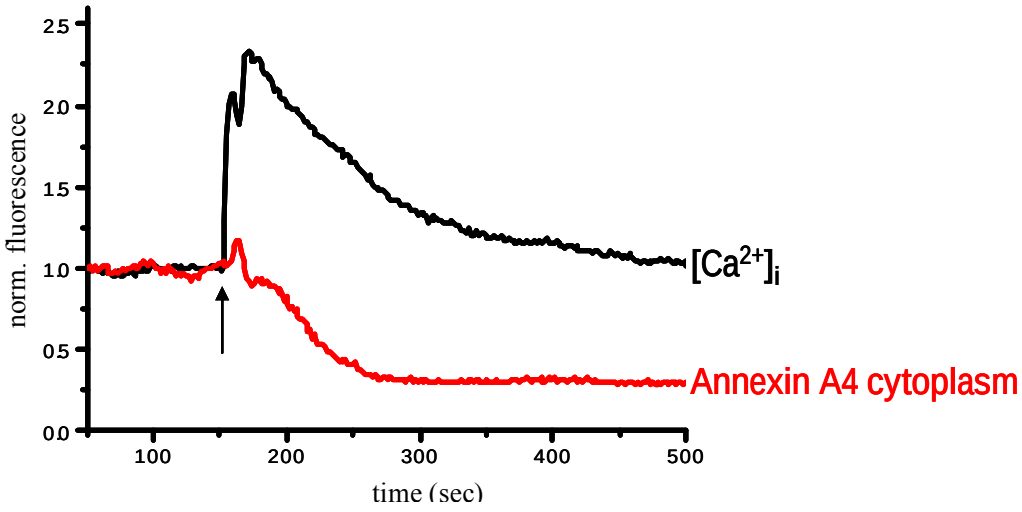

Figure S3. Calcium-dependency of annexin A4 translocation induced by ionomycin treatment or microneedle puncturing. (A) In contrast to the complete nuclear and

plasma membrane translocation of wildtype GFP-annexin A4 after addition of 5 μM ionomycin, mutated annexin A4-mCherry (E35A, D78A, D144A, E228A and D303A) showed no translocation. (B) Topographic cuts for wildtype annexin A4 (upper traces) and mutated annexin A4 (lower traces) from cell images shown in A before (red traces) and after (black trace) ionomycin treatment. Data are representative results obtained in 15 cells from 3 independent experiments. (C) Time series images of a wildtype GFP-annexin A4 and the annexin A4-mCherry mutant co-expressing HeLa cell were acquired simultaneously after wounding the cell with a glass needle. Arrows in C indicate the impact site. Data are representative results obtained in 11 cells from 4 independent experiments.

Figure S3

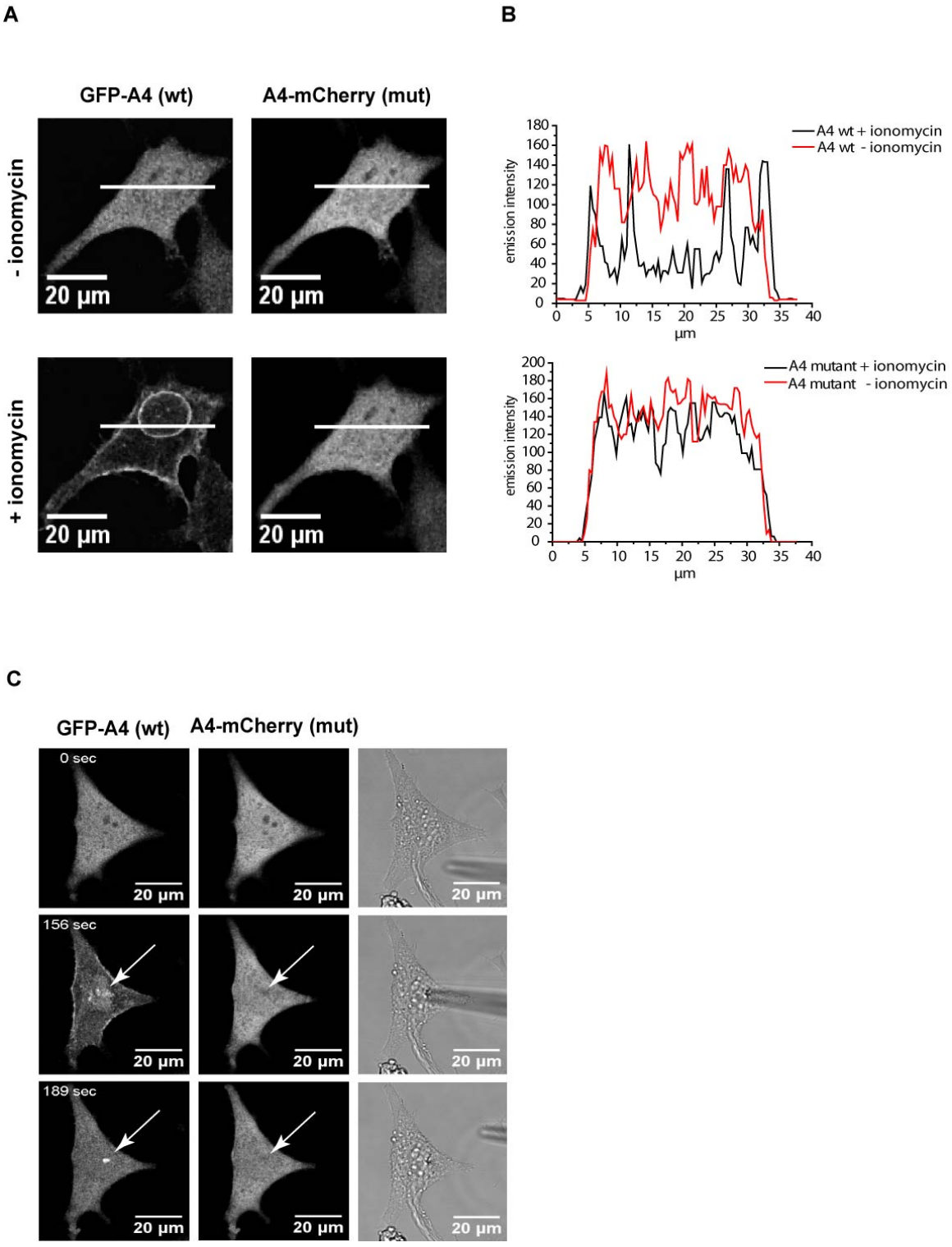

Figure S4. High resolution images of the impact site by correlative fluorescence and electron microscopy. Transmission (A) and fluorescence image (B) of the wounded cell.

The arrow shows the accumulation of annexin A4-mCherry at the impact site. The position of the wounded cell is marked by a rectangle, etched in the glass coverslip by a 532 nm pulsed laser. For excitation of mCherry the 561 nm laser line was used. Emission was collected between 580-650 nm. Scale bar 35 µm. (C-E) Close-up electron micrographs of the same wounded cell in different depth from the cell surface. Section 2 (~100 – 140 nm, C) shows the hole in the membrane and the dense packing of vesicular structures. Section 3 (~150-220 nm, D) is similar but the impact site itself is here closed. In section 6 (~ 400 – 520 nm, E) the impact region is still visible but likely represents the bottom of the 'patch'.

Figure S4

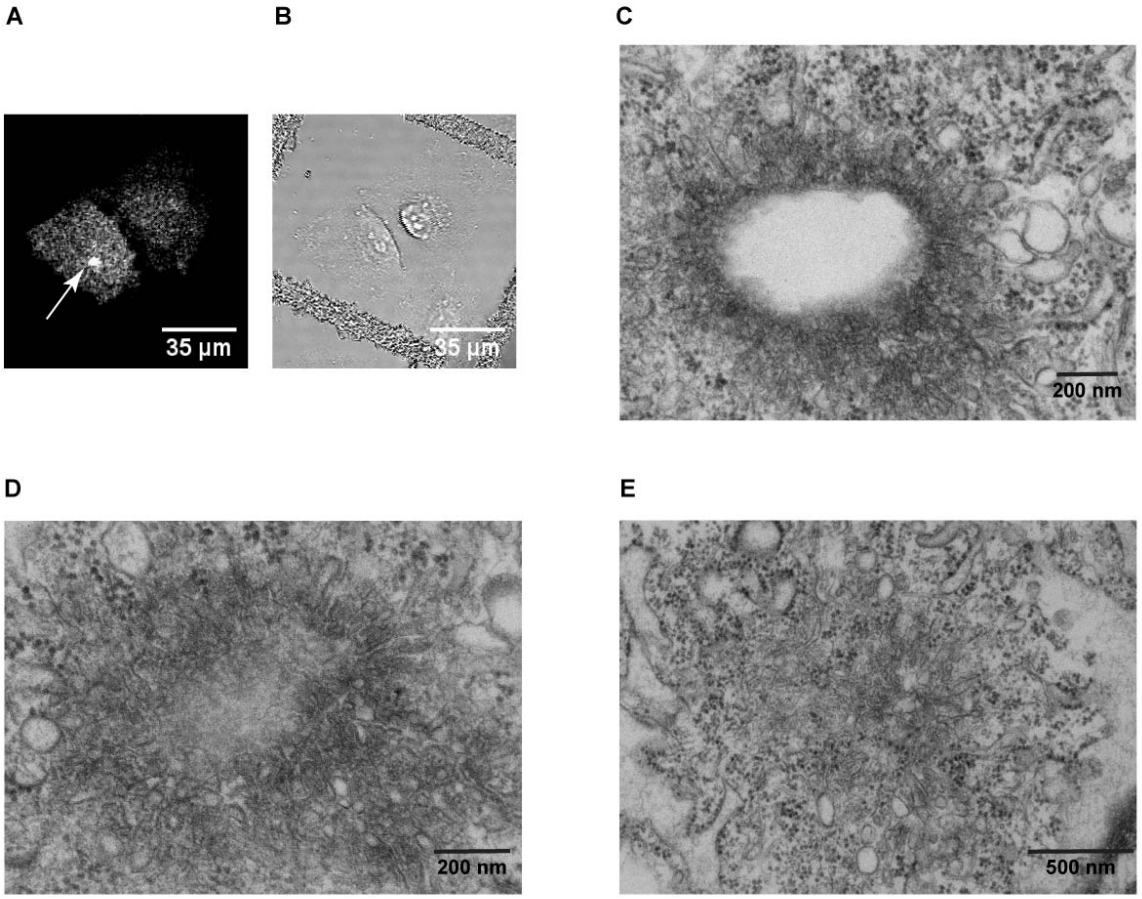

Figure S5. Immunogold electron microscopy revealed the vesicular location of aggregated annexin A4. (A) Rectangular regions in the overview electron micrograph are indicating the region of the close-up views B and C. Immunogold labelling against the GFP attached to annexin A4 shows labelling on the surface of the aggregated vesicles as well as at the rim of the impact site (B and C).

Figure S5

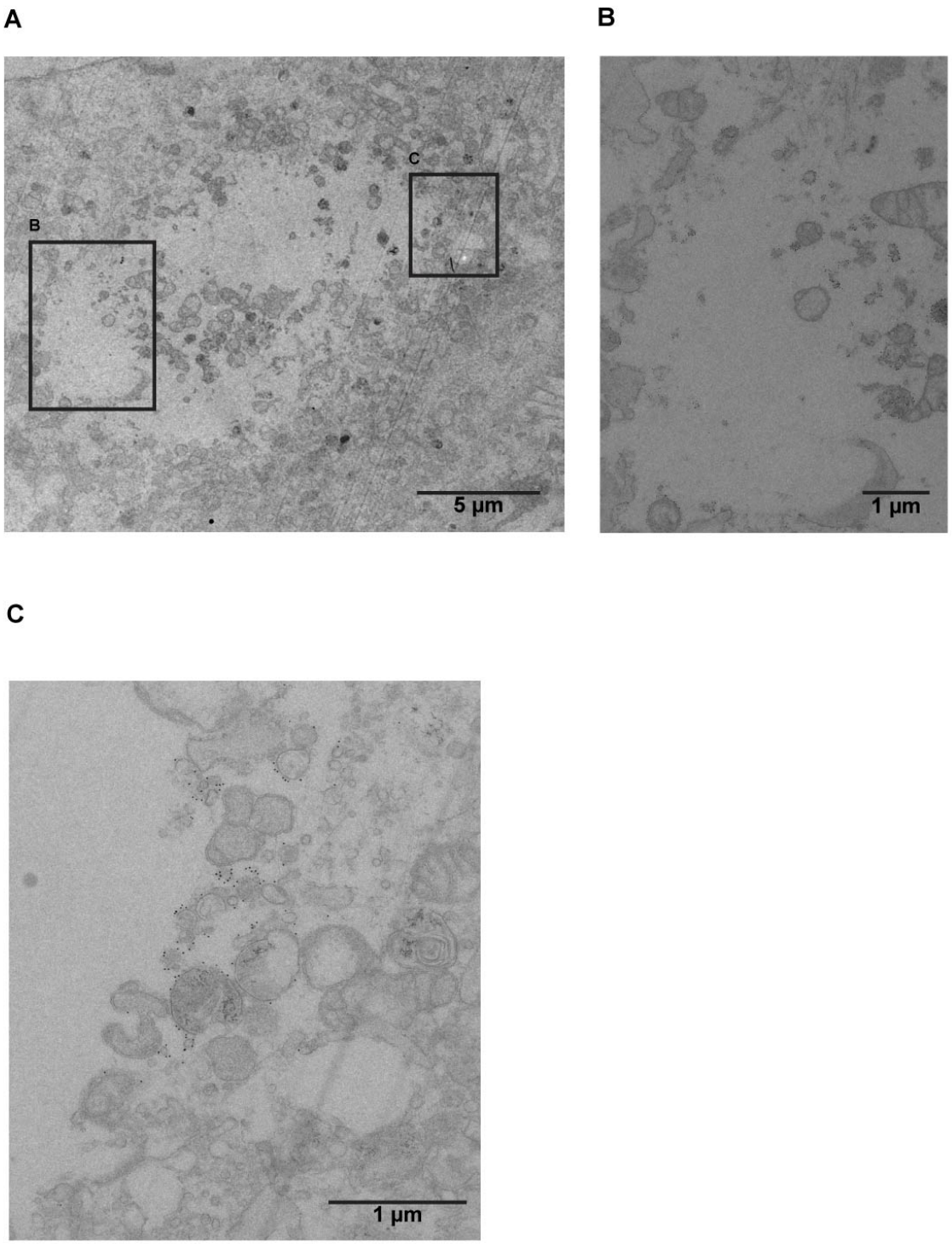

Figure S6. (A) Simultaneous recording of annexin A4-mCherry and GFP-calpain II (large subunit) and synaptotagmin VII-YFP translocation behaviour after

mechanical wounding of a HeLa cell. Arrows are indicating the impact site. In comparison to annexin A4, calpain II showed only a very weak translocation response. (B) Simultaneous recording of annexin A4-mKate and synaptotagmin VII-YFP translocation behaviour after microneedle puncturing. Arrows are indicating the impact site. In contrast to annexin A4, synaptotagmin VII shows a strong and global plasma membrane translocation.

Figure S6

A

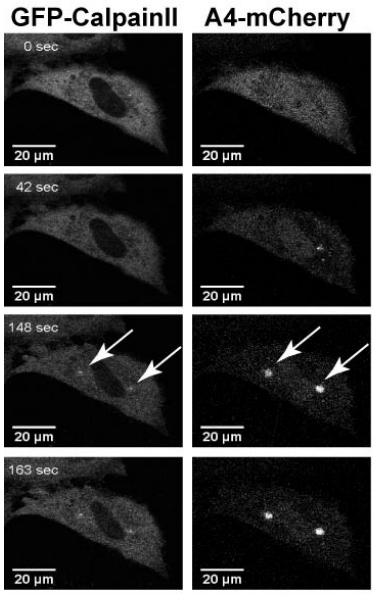
GFP-CalpainII
A4-mCherry
0 sec
42 sec
148 sec
163 sec
20 µm

B

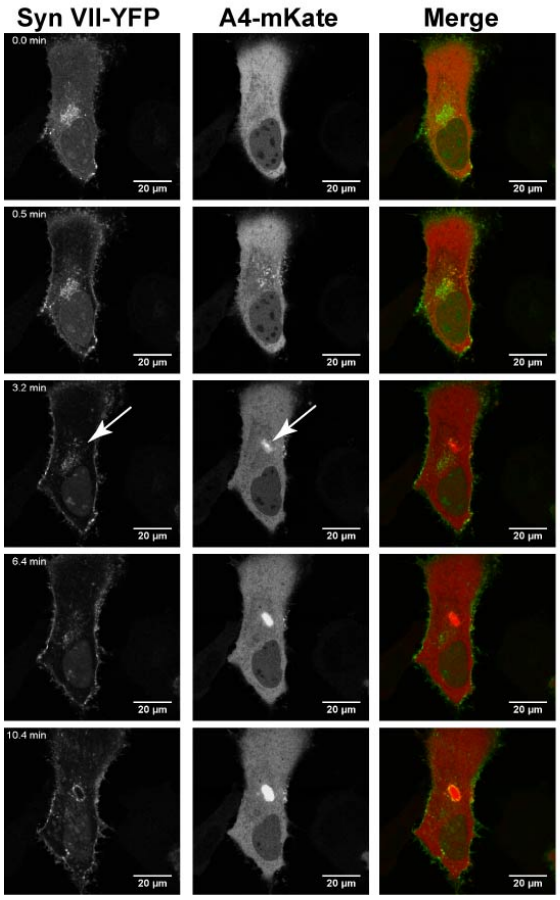
Syn VII-YFP
A4-mKate
Merge
0.0 min
0.5 min
3.2 min
6.4 min
10.4 min
20 µm

Movie S1. Simultaneous imaging of annexin A6-CFP, annexin A1-GFP and mPlum-annexin A4 translocation after microneedle puncturing in HeLa cells. Frames were taken every 3.714 seconds (display rate: 10 fps). Images were analyzed by time-lapse confocal microscopy using a laser-scanning confocal microscope (Leica TCS SP2 AOBS microcope, Leica Microsystems). Time series images shown in Figure 1A.

Movie S2. Simultaneous Fluo-4 response and annexin A4-mCherry translocation after microneedle puncturing of a HeLa cell. Frames were taken every 3.367 seconds (display rate: 10 fps). Images were analyzed by time-lapse confocal microscopy using a laser-scanning confocal microscope (Leica TCS SP2 AOBS microcope, Leica Microsystems). Time series images shown in Figure 2A.

Movie S3. PKCα-GFP and annexin A4-mKate translocation after microneedle puncturing of a HeLa. Frames were taken every 2 seconds (display rate: 10 fps). Images were analyzed by time-lapse confocal microscopy using a laser-scanning confocal microscope (Leica TCS SP2 AOBS microcope, Leica Microsystems). Time series images shown in Figure 6A.